Check for updates

Theory of isomeric excitation of ^{229}Th via electronic processes

Hanxu Zhang and Xu Wang*

Graduate School, China Academy of Engineering Physics, Beijing, China

A unified theoretical framework is presented for the isomeric excitation of the ^{229}Th nucleus via electronic processes. These processes include nuclear excitation by electron transition (NEET), nuclear excitation by electron capture (NEEC), and nuclear excitation by inelastic electron scattering (NEIES). Detailed calculation results on the excitation rate and the excitation cross section are presented.
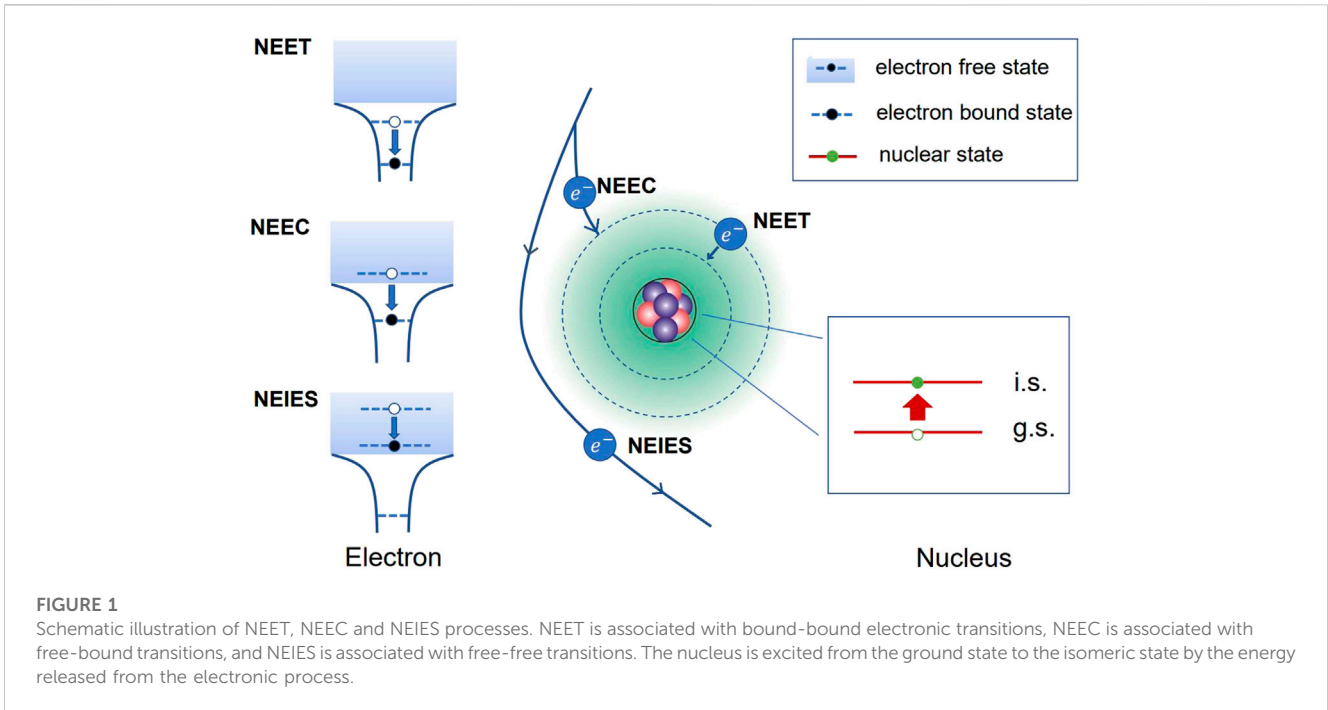
1 Introduction

In 1976, Kroger and Reich proposed that ^{229}Th has an isomeric state with energy below 100 eV (denoted as ^{229m}Th) [1]. With the development of experimental techniques, the energy of this isomeric state was estimated to be 1 ± 4 eV [2], 3.5 ± 1.0 eV [3], 7.6 ± 0.5 eV [4], and recently 8.28 ± 0.17 eV [5]. The energy of the second excited state of ^{229}Th is 29 keV. The second lowest nuclear state is the isomeric state of ^{235}U, which has an energy of 76 eV [6–8]. Therefore, ^{229m}Th is the only known nuclear excited state on the 1-eV order of magnitude, and it has attracted much attention in recent years for its potential applications in nuclear optical clocks [9–12], nuclear lasers [13], checking temporal variations of fundamental constants [14–16], etc.

These potential applications make it desirable to prepare the isomeric state in a controllable and efficient way. Currently, ^{229m}Th can be obtained from α decay of ^{233}U or β decay of ^{229}Ac [17]. The efficiency of the former decay is very low with the obtained nuclei having a recoil energy of 84 keV, and the latter decay is subject to low yield of ^{229}Ac. Direct light excitation using vacuum ultraviolet light has been attempted by several groups without success [18–21]. Possible reasons include inaccurate knowledge of the isomeric energy, competing fluorescence signals from the electrons, competition with nonradiative channels, etc. In 2019, Masuda et al. obtained this isomeric state experimentally by an indirect light excitation approach [22]. They used narrowband 29 keV synchrotron radiations to excite the ^{229}Th nuclei from the ground state to the second excited state which then decays preferably into the isomeric state [23]. Excitation processes via coupling to electrons have also been extensively studied, for example, electronic bridge (EB) processes [24–30], inelastic scattering of electrons [31, 32] or muons [33], and laser-driven electron recollision [34–36].

In the current paper we consider nuclear excitation of ^{229}Th by three different but related electronic processes. They include nuclear excitation by electron transition (NEET) [37–41], nuclear excitation by electron capture (NEEC) [42–50], and nuclear excitation by inelastic electron scattering (NEIES) [31, 32, 51, 52]. Figure 1 shows an illustration of these three processes: (a) NEET occurs when the electron transitions from a higher bound state to a lower bound state and excites the nucleus simultaneously. It was first proposed in 1973 in ^{235}U [37] and has been confirmed experimentally with ^{197}Au [38, 40]. (b) NEEC occurs when a free electron is captured by an ion and excites the nucleus with the released energy. It has

FIGURE 1
Schematic illustration of NEET, NEEC and NEIES processes. NEET is associated with bound-bound electronic transitions, NEEC is associated with free-bound transitions, and NEIES is associated with free-free transitions. The nucleus is excited from the ground state to the isomeric state by the energy released from the electronic process.

been proposed and widely discussed for a long time, mostly with ^{93}Mo. At present there are still discrepancies between theoretical calculations and experimental results, and also between different experiments [48–50]. (c) NEIES occurs when the electron transitions from a higher continuum state to a lower continuum state. It is a widely studied process in nuclear physics, almost all with high-energy electrons [52–58]. Tkalya proposes to excite ^{229}Th with low-energy electrons on the order of 10 eV [31]. We have also calculated and analyzed this process in depth in our previous work [32].

The goal of the current work is twofold. One is to provide a unified theoretical framework for the three electronic excitation processes. They are usually studied separately, but they are in fact related with differences only in the type of the initial or the final electronic states. The other goal is to present the NEET, NEEC, and NEIES results for ^{229m}Th. Although the NEIES process has been studied previously [31, 32], results of NEET or NEEC have not been reported for ^{229}Th in the literature, as far as we are aware of. Our results presented here can be directly used for the excitation of ^{229}Th in complex environments, such as plasmas, beam collisions, etc.

2 Theoretical framework

2.1 Transition rate

The common point of NEET, NEEC, and NEIES is that the electron transitions from a state with higher energy to a state with lower energy, and the nucleus is excited simultaneously with the released energy. No photons are emitted during these processes. The system (consisting of a nucleus, an electron, and a quantized radiation field) transitions from an initial state $|i\rangle$ ($t = t_i$) to a

final state $|f\rangle$ ($t = t_f$) under the effect of an interaction Hamiltonian V. The time evolution operator of the system is given as

$$U(t_f, t_i) \equiv \mathcal{P}e^{\left[\frac{1}{i\hbar}\int_{t_i}^{t_f} V_I(t)dt\right]},$$
(1)

where $\mathcal{P}$ is the chronological operator, and $V_I(t)$ is V in the interaction picture,

$$V_I(t) = e^{\frac{i}{\hbar}H_0 t} V e^{-\frac{i}{\hbar}H_0 t}.$$
(2)

Expand the time evolution operator and assume the following three conditions: (a) $|i\rangle \neq |f\rangle$; (b) $t_i = 0$, $t_f = \infty$; and (c) the initial and final states have a total dissipation rate Γ_t, so the time evolution of the wave function is multiplied by $e^{-\Gamma_t t/2}$. After integrating over time, the transition matrix element can be written as

$$T_{fi} = U_{fi} - I_{fi} = V_{fi}\frac{1}{(E_f - E_i) + i\Gamma_t/2},$$
(3)

where I is the unit operator. The transition rate can be given as the transition probability divided by the lifetime $\tau = 1/\Gamma_t$ of the system

$$\omega_{fi} = 2\pi|V_{fi}|^2 L_t(E_f - E_i),$$
(4)

where L_t is a normalized Lorenzian function

$$L_t(E_f - E_i) = \frac{\Gamma_t/2\pi}{(E_f - E_i)^2 + \Gamma_t^2/4}.$$
(5)

Consider the on-shell condition of $E_i = E_f$, and if the dissipation in the system or the subsequent decay process can be ignored, then Γ_t approaches 0, and the Lorenzian reduces to the Dirac-δ function

$$\omega_{fi} = 2\pi|V_{fi}|^2\delta(E_f - E_i).$$
(6)

Given the interaction operator V and the initial and final states of the system, the interaction matrix element V_{fi} can be calculated. Then the transition rate can then be obtained with Eq. 4 or Eq. 6.

2.2 Initial and final states

The system under consideration consists of a nucleus, an electron, and a quantized radiation field. The total Hamiltonian can be written as

$$H = H_0 + V = H_n + H_e + H_{rad} + V, \tag{7}$$

where H_n is the Hamiltonian for the nucleus, H_e for the electron, and H_{rad} for the radiation field. V is the interaction Hamiltonian. The initial state $|i\rangle$ and the final state $|f\rangle$ are eigenstates of H_0.

The state of the total system is written as the product of the states of the nucleus $|IM\rangle$, of the electron $|\phi\rangle$, and of the radiation field with n optical quanta $|n\rangle$:

$$\begin{aligned} |i\rangle &= |I_i M_i\rangle \otimes |\phi_i\rangle \otimes |0\rangle, \\ |f\rangle &= |I_f M_f\rangle \otimes |\phi_f\rangle \otimes |0\rangle. \end{aligned} \tag{8}$$

Here $I_{i,f}$ and $M_{i,f}$ are the total angular momentum and the magnetic quantum number of the initial or the final state of the nucleus.

For the nuclear part, the initial state is the nuclear ground state with energy, $E_g = 0$ eV and spin parity $I_g^+ = 5/2^+$, and the final state is the isomeric state with energy $E_{is} = 8.28$ eV and spin parity $I_{is}^+ = 3/2^+$. For the radiation-field part, both the initial and the final state is $|0\rangle$ (viz. the vacuum state) because the processes have no absorption and emission of real photons. Exchanging of virtual photons happens between the electron and the nucleus in intermediate states.

The electronic wave functions are eigenstates of the time-independent Dirac equation

$$[-ic\boldsymbol{\alpha} \cdot \nabla + \beta c^2 + \mathcal{V}_{Th}(r)]|\phi\rangle = \mathcal{E}|\phi\rangle, \tag{9}$$

where $\mathcal{V}_{Th}(r) = \mathcal{V}_{nu}(r) + \mathcal{V}_{el}(r)$ is the potential energy felt by the electron, which is provided by the ^{229}Th nucleus and the atomic electron cloud. The potential energies have the form

$$\begin{aligned} \mathcal{V}_{nu}(r) &= -\int \frac{\rho_{nu}(r')}{|\boldsymbol{r} - \boldsymbol{r}'|}\,d\tau', \\ \mathcal{V}_{el}(r) &= -\int \frac{\rho_{el}(r')}{|\boldsymbol{r} - \boldsymbol{r}'|}\,d\tau', \end{aligned}$$

$\rho_{nu/el}$ is the charge density of the nucleus/electron shell.

For the NEET process, $|\phi_i\rangle$ and $|\phi_f\rangle$ are both Dirac bound states with the form

$$|\phi\rangle = |n\eta m\rangle = \begin{pmatrix} g_{n\eta}(r)\Omega_{\eta m}(\hat{\boldsymbol{r}}) \\ -if_{n\eta}(r)\Omega_{-\eta m}(\hat{\boldsymbol{r}}) \end{pmatrix}, \tag{10}$$

where $g_{n\eta}(r)$ and $f_{n\eta}(r)$ are radial wave functions, n is the principal quantum number, η is a notation determined by the total angular momentum j and the orbital angular momentum l, and m is the magnetic quantum number of j. η is given by

$$\eta = (l - j)(2j + 1). \tag{11}$$

For $\eta < 0$, l should be changed to $l' = 2j - l$. $\Omega_{\eta m}$ are spherical spinors

$$\Omega_{\eta m}(\hat{\boldsymbol{r}}) \equiv \Omega_{jlm}(\hat{\boldsymbol{r}}) = \sum_{\nu=\pm 1/2} \langle l, 1/2, j|m - \nu, \nu, m\rangle Y_{l,m-\nu}(\hat{\boldsymbol{r}})\chi^\nu, \tag{12}$$

where χ^ν is

$$\chi^{1/2} = \begin{pmatrix} 1 \\ 0 \end{pmatrix} \quad \text{and} \quad \chi^{-1/2} = \begin{pmatrix} 0 \\ 1 \end{pmatrix}. \tag{13}$$

For the NEIES process, $|\phi_i\rangle$ and $|\phi_f\rangle$ are both Dirac scattering states, which can be expanded into partial wave series [59, 60]:

$$\begin{aligned} |\phi\rangle &= |\boldsymbol{k}\nu\rangle^{(\pm)} \\ &= \frac{4\pi}{k}\sqrt{\frac{\mathcal{E} + m_e c^2}{2\mathcal{E}}} \sum_{\eta m} \left[\Omega_{\eta m}^\dagger(\hat{\boldsymbol{k}})\chi^\nu\right] e^{\pm id_{\mathcal{E}\eta}} \begin{pmatrix} g_{\mathcal{E}\eta}(r)\Omega_{\eta m}(\hat{\boldsymbol{r}}) \\ -if_{\mathcal{E}\eta}(r)\Omega_{-\eta m}(\hat{\boldsymbol{r}}) \end{pmatrix}. \end{aligned} \tag{14}$$

The initial state (before scattering) takes the plus sign and the final state (after scattering) takes the minus sign: $|\phi_i\rangle = |\boldsymbol{k}_i\nu_i\rangle^{(+)}$ and $|\phi_f\rangle = |\boldsymbol{k}_f\nu_f\rangle^{(-)}$. $\boldsymbol{k}$ is the wave vector. $d_{\mathcal{E}\eta}$ is the total phase shift.

For the NEEC process, $|\phi_i\rangle$ is a Dirac scattering state and $|\phi_f\rangle$ is a Dirac bound state.

2.3 The interaction matrix element

The interaction Hamiltonian V is given by

$$V = -\frac{1}{c}\int [\boldsymbol{j}_n(\boldsymbol{r}) + \boldsymbol{j}_e(\boldsymbol{r})] \cdot \mathbf{A}(\boldsymbol{r})d\tau + \int \frac{\rho_n(\boldsymbol{r})\rho_e(\boldsymbol{r}')}{|\boldsymbol{r} - \boldsymbol{r}'|}d\tau d\tau', \tag{15}$$

where the first integral is the couplings between the nuclear current density $\boldsymbol{j}_n$ and the electron current density $\boldsymbol{j}_e$ with the vector potential $\mathbf{A}$ of the radiation field. The second integral is the Coulomb interaction between the nucleus and the electron, with ρ_n and ρ_e being the charge density operator of the nucleus and of the electron, respectively. The vector potential of the radiation field can be expanded in multipole components as

$$\begin{aligned} \mathbf{A}(\boldsymbol{r}) = \sum_{\lambda\mu q} &[a(E\lambda, \mu, q)\boldsymbol{A}(E\lambda, \mu, q) \\ &+ a(M\lambda, \mu, q)\boldsymbol{A}(M\lambda, \mu, q) + h.c.]. \end{aligned} \tag{16}$$

In the above expression, λ, μ, q are the angular momentum quantum number, magnetic quantum number, and wave number, respectively, and

$$\begin{aligned} \boldsymbol{A}(E\lambda, \mu, q) &= \sqrt{\frac{8\pi c^2}{\lambda(\lambda + 1)R}}\nabla \times \boldsymbol{L}\left[j_\lambda(qr)Y_{\lambda\mu}(\theta, \phi)\right], \\ \boldsymbol{A}(M\lambda, \mu, q) &= i\sqrt{\frac{8\pi c^2 q^2}{\lambda(\lambda + 1)R}}\boldsymbol{L}\left[j_\lambda(qr)Y_{\lambda\mu}(\theta, \phi)\right]. \end{aligned} \tag{17}$$

Here R is the radius of the spherical volume under consideration, $\boldsymbol{L}$ is the angular momentum operator, $j_\lambda(qr)$ is a spherical Bessel function, and $Y_{\lambda\mu}$ is the spherical harmonics. The expansion coefficient a and its conjugate are the operators for photon annihilation and creation. The matrix elements of these operators are

$$\langle n|a|n + 1\rangle = \langle n + 1|a^\dagger|n\rangle = \sqrt{\frac{n + 1}{2qc}} \tag{18}$$

where $|n\rangle$ represents a number state with n photons.

Using Eq. 8 and Eqs 15–18, the transition matrix element V_{fi} can be obtained [61]

$$V_{fi} = \sum_{\lambda\mu} \frac{4\pi}{2\lambda+1}(-1)^\mu \Big\{ \langle\phi_f|\mathcal{N}(E\lambda,\mu)|\phi_i\rangle\langle I_f M_f|\mathcal{M}(E\lambda,-\mu)|I_i M_i\rangle$$
$$-\langle\phi_f|\mathcal{N}(M\lambda,\mu)|\phi_i\rangle\langle I_f M_f|\mathcal{M}(M\lambda,-\mu)|I_i M_i\rangle\Big\},$$
(19)

where $\mathcal{M}(\mathcal{T}\lambda,\mu)$ and $\mathcal{N}(\mathcal{T}\lambda,\mu)$ are the electric ($\mathcal{T}=E$) or magnetic ($\mathcal{T}=M$) multipole transition operators of the nucleus and of the electron, respectively:

$$\mathcal{M}(E\lambda,\mu) = \frac{(2\lambda+1)!!}{\kappa^{\lambda+1}c(\lambda+1)}\int \boldsymbol{j}_n\cdot\nabla\times\boldsymbol{L}\big[j_\lambda(\kappa r)Y_{\lambda\mu}(\theta,\phi)\big]d\tau,$$
(20)

$$\mathcal{M}(M\lambda,\mu) = \frac{-i(2\lambda+1)!!}{\kappa^\lambda c(\lambda+1)}\int \boldsymbol{j}_n\cdot\boldsymbol{L}\big[j_\lambda(\kappa r)Y_{\lambda\mu}(\theta,\phi)\big]d\tau, \quad (21)$$

$$\mathcal{N}(E\lambda,\mu) = \frac{i\kappa^\lambda}{c\lambda(2\lambda-1)!!}\int \boldsymbol{j}_e\cdot\nabla\times\boldsymbol{L}\big[h_\lambda^{(1)}(\kappa r)Y_{\lambda\mu}(\theta,\phi)\big]d\tau,$$
(22)

$$\mathcal{N}(M\lambda,\mu) = \frac{\kappa^{\lambda+1}}{c\lambda(2\lambda-1)!!}\int \boldsymbol{j}_e\cdot\boldsymbol{L}\big[h_\lambda^{(1)}(\kappa r)Y_{\lambda\mu}(\theta,\phi)\big]d\tau. \quad (23)$$

In the above formulas $\kappa = \Delta E/c$ with $\Delta E = 8.28$ eV being the energy of the isomeric state, and $h_\lambda^{(1)}(\kappa r)$ is the spherical Hankel function of the first kind. For $\kappa r \ll 1$ the asymptotic form $h_\lambda^{(1)}(\kappa r) \approx -i(2\lambda-1)!!/(\kappa r)^{\lambda+1}$ may be used [62].

2.4 Nuclear excitation rate and cross section

2.4.1 NEET rate

For NEET, the initial and final states of the electron may have spontaneous radiation, and the isomeric state of the nucleus has an internal conversion rate and a radiation decay rate. Thus, Γ_t in Eq. 5 will be $\Gamma_{\text{NEET}} = \Gamma_i + \Gamma_f + \Gamma_n$, where $\Gamma_{i/f}$ is the spontaneous emission rate of electronic state, $\Gamma_n = \Gamma_{\text{IC}} + \Gamma_\gamma$ is the natural width of the isomeric state, with Γ_{IC} being the internal conversion rate and Γ_γ being the radiation decay rate.

Introduce reduced nuclear transition probabilities

$$B(\mathcal{T}\lambda; I_i \to I_f) = \frac{1}{2I_i+1}\sum_{M_f M_i \mu}|\langle I_f M_f|\mathcal{M}(\mathcal{T}\lambda,\mu)|I_i M_i\rangle|^2.$$
(24)

With Eqs 10, 19, averaging over initial states and summing over final states, the modulus square of the matrix element in Eq. 4 becomes

$$|V_{fi}|^2 = 4\pi\sum_{\mathcal{T}\lambda}\Big[B(\mathcal{T}\lambda; I_i \to I_f)\frac{\kappa^{2\lambda+2}}{(2\lambda+1)!!^2}\big(C_{j_i 1/2\lambda 0}^{j_f 1/2}\big)^2|M_{fi}^{\mathcal{T}\lambda}|^2\Big],$$
(25)

where $C_{j_i 1/2\lambda 0}^{j_f 1/2}$ is a Clebsch-Gordan coefficient with the relation

$$\big(C_{j_i 1/2\lambda 0}^{j_f 1/2}\big)^2 = (2l_i+1)(2l_f+1)$$
$$\times(2j_f+1)\begin{pmatrix} l_i & \lambda & l_f \\ 0 & 0 & 0 \end{pmatrix}^2 \begin{Bmatrix} l_i & \lambda & l_f \\ j_f & 1/2 & j_i \end{Bmatrix}^2, \quad (26)$$

and $M_{fi}^{\mathcal{T}\lambda}$ are radial matrix elements given by

$$M_{fi}^{E\lambda} = \int_0^\infty h_\lambda^{(1)}(\kappa r)\big[g_i(r)g_f(r)+f_i(r)f_f(r)\big]r^2 dr - \int_0^\infty h_{\lambda-1}^{(1)}(\kappa r)$$
$$\times\Big[\frac{(\eta_i-\eta_f+\lambda)}{\lambda}g_f(r)f_i(r)+\frac{(\eta_i-\eta_f-\lambda)}{\lambda}f_f(r)g_i(r)\Big]r^2 dr,$$

$$M_{fi}^{M\lambda} = \frac{\eta_i+\eta_f}{\lambda}\int_0^\infty h_\lambda^{(1)}(\kappa r)\big[g_i(r)f_f(r)+g_f(r)f_i(r)\big]r^2 dr.$$
(27)

For $M\lambda$ type transition, one needs to change $l_i \to l_i'$ in Eq. 26. For $\kappa \ll 1$, the $h_{\lambda-1}^{(1)}$ term in Eq. 27 can be neglected, since $h_{\lambda-1}^{(1)}(\kappa r) \ll h_\lambda^{(1)}(\kappa r)$ for low energy transitions.

With Eq. 4 and Eq. 25, we obtain the transition rate of NEET

$$\omega_{\text{NEET}} = 4\pi\sum_{\mathcal{T}\lambda}\Big[B(\mathcal{T}\lambda; I_i \to I_f)\frac{\kappa^{2\lambda+2}}{(2\lambda+1)!!^2}\big(C_{j_i 1/2\lambda 0}^{j_f 1/2}\big)^2|M_{fi}^{\mathcal{T}\lambda}|^2\Big]$$
$$\times\frac{\Gamma_{\text{NEET}}}{(E_f-E_i)^2+\Gamma_{\text{NEET}}^2/4}.$$
(28)

Here, $E_i = \mathcal{E}_i$, $E_f = \mathcal{E}_f + E_{\text{is}}$. In case of resonant condition, $\mathcal{E}_i = \mathcal{E}_f + 8.28$ eV. This applies for NEET, NEEC and NEIES.

2.4.2 NEEC cross section

The excitation rate for the NEEC process can also be derived from Eq. 4, except that Γ_t will be different, since the initial state is now a free state. If the electron is captured into the ionic ground state, then $\Gamma_{\text{NEEC}} = \Gamma_n$. Otherwise $\Gamma_{\text{NEEC}} = \Gamma_f + \Gamma_n$. With Eqs. 10, 14, 19, 24, the modulus square of the interaction matrix element becomes

$$|V_{fi}|^2 = 4\pi^2\frac{\mathcal{E}_i+m_e c^2}{\mathcal{E}_i p_i^2}\sum_{\mathcal{T}\lambda}B(\mathcal{T}\lambda; I_i \to I_f)\frac{\kappa^{2\lambda+2}}{(2\lambda+1)!!^2}$$
$$\times\sum_{\eta_i}(2j_i+1)\big(C_{j_i 1/2\lambda 0}^{j_f 1/2}\big)^2|M_{fi}^{\mathcal{T}\lambda}|^2.$$
(29)

The excitation cross section can be defined through $\omega = \sigma j$, with j being the flux of the initial free state

$$\sigma_{\text{NEEC}}(\mathcal{E}_i) = \frac{4\pi^2}{c^2}\frac{\mathcal{E}_i+m_e c^2}{p_i^3}\sum_{\mathcal{T}\lambda}\Big[B(\mathcal{T}\lambda; I_i \to I_f)\frac{\kappa^{2\lambda+2}}{(2\lambda+1)!!^2}$$
$$\times\sum_{\eta_i}(2j_i+1)\big(C_{j_i 1/2\lambda 0}^{j_f 1/2}\big)^2|M_{fi}^{\mathcal{T}\lambda}|^2\frac{\Gamma_{\text{NEEC}}}{(E_i-E_f)^2+\Gamma_{\text{NEEC}}^2/4}\Big].$$
(30)

Γ_{NEEC} is usually very small so the Lorenzian can be approximated as the Dirac-δ function, which has been referred as the isolated resonance approximation [46]. Generally speaking, if the energy of the incoming electron has a certain distribution, it is often necessary to integrate over the energy of the free electron. The so-called resonant strength is defined to simplify the calculation

$$S = \int d\mathcal{E}_i\ \sigma_{\text{NEEC}}(\mathcal{E}_i).$$
(31)

2.4.3 NEIES cross section

For NEIES, Fermi's Golden Rule can be obtained by summing over the final energy states of the electron with Eq. 6

$$\frac{d\sigma}{d\Omega} = \frac{2\pi}{v_i} \rho(\mathcal{E}_f)|V_{fi}|^2, \tag{32}$$

where Ω is the solid angle of the outgoing direction, $v_i = p_i c^2/\mathcal{E}_i$ is the asymptotic incoming speed, $\rho(\mathcal{E}_f) = p_f \mathcal{E}_f/(8\pi^3 c^2)$ is the density of the final states, $\mathcal{E}_{i,f} = \sqrt{p_{i,f}^2 c^2 + m_e^2 c^4}$ is the energy of the initial or the final state.

With Eq. 14 and 19 and Eq. 24, averaging over initial states and summing over final states, the modulus square of the interaction matrix element becomes

$$|V_{fi}|^2 = 32\pi^4 \frac{\mathcal{E}_f + m_e c^2}{\mathcal{E}_f \, p_f^2} \frac{\mathcal{E}_i + m_e c^2}{\mathcal{E}_i \, p_i^2}$$
$$\times \sum_{\mathcal{T}\lambda}\left[B(\mathcal{T}\lambda, I_i \to I_f) \frac{\kappa^{2\lambda+2}}{(2\lambda+1)!!^2} \sum_{\eta_i,\eta_f}(2j_i+1)\left(C_{j_i 1/2\lambda 0}^{j_f 1/2}\right)^2 |M_{fi}^{\mathcal{T}\lambda}|^2 \right]. \tag{33}$$

And the total NEIES cross section is

$$\sigma_{\text{NEIES}}(\mathcal{E}_i) = \frac{8\pi^2}{c^4} \frac{p_f}{p_i} \frac{\mathcal{E}_f + m_e c^2}{p_f^2} \frac{\mathcal{E}_i + m_e c^2}{p_i^2}$$
$$\times \sum_{\mathcal{T}\lambda}\left[B(\mathcal{T}\lambda, I_i \to I_f) \frac{\kappa^{2\lambda+2}}{(2\lambda+1)!!^2} \sum_{\eta_i,\eta_f}(2j_i+1)\left(C_{j_i 1/2\lambda 0}^{j_f 1/2}\right)^2 |M_{fi}^{\mathcal{T}\lambda}|^2 \right]. \tag{34}$$

3 Numerical results

In this section, we present calculation results of ^{229m}Th excited via NEET, NEEC, and NEIES. For the ^{229}Th nucleus, the spin parity of the ground state is $5/2^+$ and that of the isomeric state is $3/2^+$, so the transition type is magnetic dipole ($M1$) or electronic quadrupole ($E2$). Relevant information about the nuclear transition matrix elements is packed in the reduced nuclear transition probabilities. There are some degree of uncertainties (roughly by a factor of two) with them, because they are obtained from model calculations or experimental analyses with approximations, for example, calculations in the framework of a quasiparticle-phonon model with inclusion of Coriolis couplings [63, 64], or experimental data analyses [65–68] exploiting Alaga rules [69, 70]. *Ab initio* calculations of $B(E2/M1)$ for a nucleus like ^{229}Th are out of reach in the foreseeable future, and there is no conclusive means to judge which set of values is better than other sets. In this paper, we use the values suggested by Minkov and Pálffy in 2017 [71]

$$B(E2, \text{is} \to \text{g}) = 27 \text{ W.u.}$$
$$B(M1, \text{is} \to \text{g}) = 0.0076 \text{ W.u.} \tag{35}$$

where W.u. stands for Weisskopf units. Note that the direction of nuclear transition has the relation

$$\frac{B(E2/M1; \text{g} \to \text{is})}{B(E2/M1; \text{is} \to \text{g})} = \frac{2I_{\text{is}}+1}{2I_{\text{g}}+1} = \frac{2}{3}. \tag{36}$$

According to Eq. 28 and 30 and Eq. 34, the calculation of the transition rate or the cross section eventually reduces to the calculation of electron radial wave functions in Eq. 27. In this paper, all calculations involving the electron radial wave functions, including the spontaneous emission rates, are performed using the code RADIAL [72] with the Dirac-Hartree-Fock-Slater method [73, 74] and a Fermi charge distribution for the nucleus.

3.1 NEET rate

NEET occurs when the energy difference between two electronic bound states matches the nuclear isomeric energy $\Delta E = E_{\text{is}} - E_{\text{g}} = 8.28$ eV. The finite widths of the initial and final states allow transitions to occur when there is a little mismatch of energy. The bigger the energy mismatch, the smaller the excitation rate. For ^{229m}Th, the half-life is 7 ± 1 μs ($\Gamma_{\text{IC}} \approx 10^{-11}$ eV) via internal conversion [75] and about 1880 s ($\Gamma_\gamma \approx 10^{-19}$ eV) via γ decay [76], while the half-life of the electronic state is typically on the order of 1–10 ns ($\Gamma_{i/f} \approx 10^{-8} - 10^{-7}$ eV). Therefore, usually $\Gamma_{i/f} \gg \Gamma_{\text{IC}} \gg \Gamma_\gamma$.

Because $\Gamma_{\text{NEET}} \approx \Gamma_i + \Gamma_f$ is on the order of 10^{-8} eV, the width of the Lorenzian is very narrow. To ensure a nonnegligible excitation rate, we try to find $\phi_i - \phi_f$ pairs that satisfy: (i) the energy constraint $|\mathcal{E}_i - \mathcal{E}_f - 8.28| < 0.1$ eV, and (ii) the angular-momentum constraint that this channel can excite the nucleus through $M1$ or $E2$ transitions.

The first ionization energy of neutral ^{229}Th is 6.3 eV, so NEET can not occur in neutral ^{229}Th. The energy levels of ^{229}Th with different ionic states are also different. As listed in Table 1, for ^{229}Th^{1+}, a single transition $7p_{3/2} \to 5f_{5/2}$ is found satisfying both constraints ($|\mathcal{E}_i - \mathcal{E}_f - 8.28| = 0.03$ eV, $M1$ and $E2$ transitions). Using Eq. 25

$$|V_{fi}|^2(7p_{3/2} \to 5f_{5/2}) = 1.53 \times 10^{-20} \text{ a.u.} \tag{37}$$

The initial electronic state $7p_{3/2}$ can decay via spontaneous emission, the rate of which is calculated to be $\Gamma_i = 3.76 \times 10^{-9}$ a. u., corresponding to a lifetime of 6.4 ns. The final state $5f_{5/2}$ does not have a spontaneous emission channel. For the nuclear part, the IC channel is closed because the energy of the final electronic state $5f_{5/2}$ is below −8.28 eV. The γ decay rate Γ_γ (= 1.28×10^{-20} a. u.) is negligible due to the very long lifetime. Therefore for this NEET channel $\Gamma_{\text{NEET}} \approx \Gamma_i = 3.76 \times 10^{-9}$ a. u., and the rate of NEET is calculated to be

$$\omega(7p_{3/2} \to 5f_{5/2}) = 2.02 \times 10^{-6} \text{ s}^{-1}. \tag{38}$$

This value is the rate of NEET for a single ^{229}Th$^+$ ion assuming that the ion is prepared in the $7p_{3/2}$ initial state.

Similar calculations can be performed for the ^{229}Th^{2+} ion and the ^{229}Th^{3+} ion. For the ^{229}Th^{2+} ion, four NEET channels are found satisfying the above two constraints, as listed in Table 2. For the ^{229}Th^{3+} ion, more than 20 NEET channels are found satisfying the above two constraints. However, most of them contribute little. Table 3 lists the seven channels with the largest NEET rate.

3.2 NEEC cross section

The NEEC cross sections are calculated with Eq. 30. Figure 2A presents the largest 10 NEEC channels of ^{229}Th$^{1+,2+,3+}$ ions. The peak values of these dominant channels are on the order of 10^3 to 10^9 b. The highest one shown by the inset corresponds to electron capture into the ground state ($7s_{1/2}$) of the ^{229}Th^{1+} ion, which has no spontaneous emission channel. In this case, $\Gamma_{\text{NEEC}} = \Gamma_{\text{IC}} = 8 \times 10^{-11}$ eV. It should be pointed out that each line in Figure 2A is actually a Lorenzian with a relatively narrow width, as illustrated by the inset. The peak represents the resonant condition $\mathcal{E}_i - \mathcal{E}_f = 8.28$
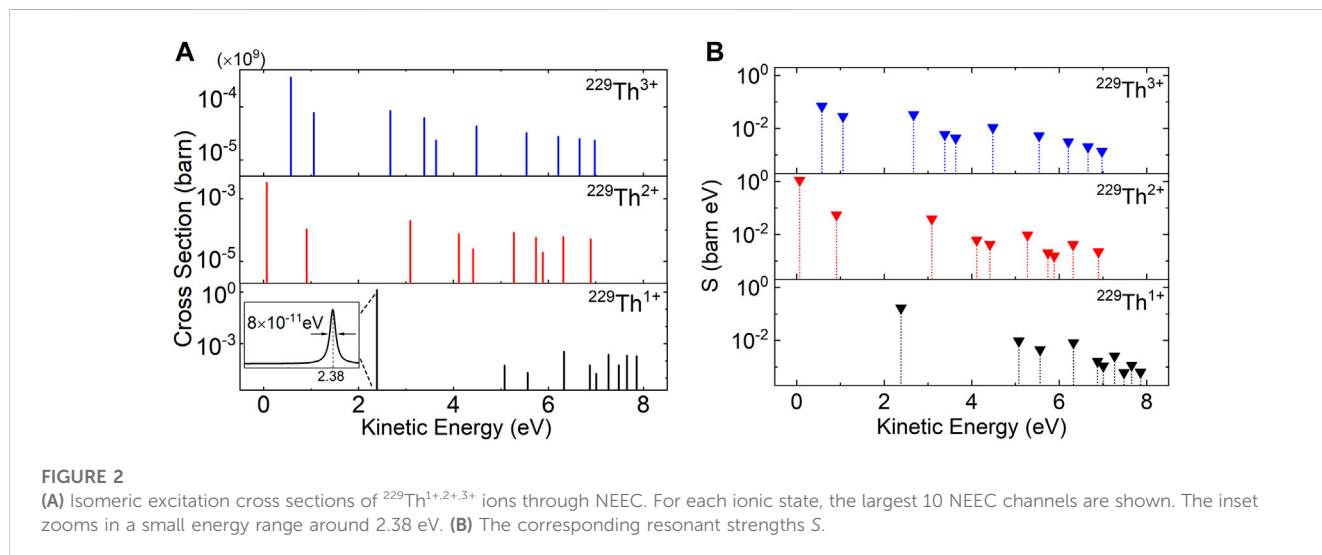
TABLE 1 NEET channels in ^{229}Th^{1+}.

ϕ_i	ϕ_f	Type	$|\mathcal{E}_i - \mathcal{E}_f - 8.28|$ (eV)	$|V_{fi}|^2$ (a.u.)	Γ_{NEET} ($\times 10^{-8}$ a.u.)	ω_{NEET} (s^{-1})
$7p_{3/2}$	$5f_{5/2}$	$M1, E2$	0.03	1.53×10^{-20}	0.376	2.02×10^{-6}

TABLE 2 NEET channels in ^{229}Th^{2+}.

ϕ_i	ϕ_f	Type	$|\mathcal{E}_i - \mathcal{E}_f - 8.28|$ (eV)	$|V_{fi}|^2$ (a.u.)	Γ_{NEET} ($\times 10^{-8}$ a.u.)	ω_{NEET} (s^{-1})
$9p_{3/2}$	$7p_{3/2}$	$M1, E2$	0.025	6.78×10^{-16}	2.52	0.87
$15d_{3/2}$	$8s_{1/2}$	$M1, E2$	0.012	4.14×10^{-19}	1.49	1.3×10^{-3}
$15d_{5/2}$	$8s_{1/2}$	$E2$	0.0076	6.92×10^{-22}	1.47	5.42×10^{-6}
$16s_{1/2}$	$8s_{1/2}$	$M1$	0.032	3.39×10^{-15}	1.54	1.57

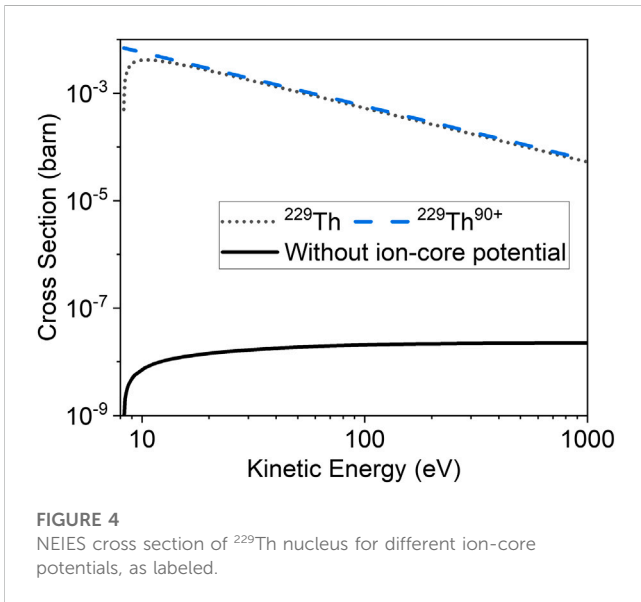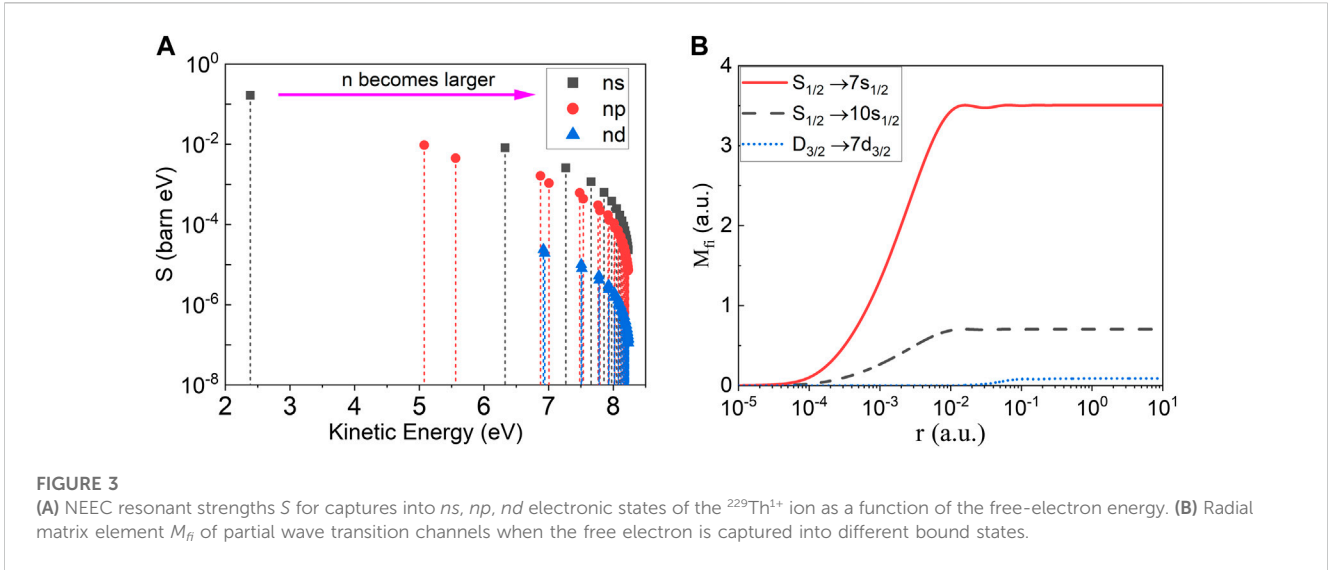**TABLE 3 NEET channels in ^{229}Th^{3+}.**

ϕ_i	ϕ_f	Type	$|\mathcal{E}_i - \mathcal{E}_f - 8.28|$ (eV)	$|V_{fi}|^2$ (a.u.)	Γ_{NEET} ($\times 10^{-8}$ a.u.)	ω_{NEET} (s^{-1})
$12p_{3/2}$	$8p_{3/2}$	$M1, E2$	0.055	1.70×10^{-16}	2.11	0.037
$24s_{1/2}$	$9s_{1/2}$	$M1$	0.037	8.15×10^{-16}	3.28	0.604
$25s_{1/2}$	$9s_{1/2}$	$M1$	0.014	7.04×10^{-16}	3.27	0.075
$24d_{3/2}$	$9s_{1/2}$	$M1, E2$	0.016	8.95×10^{-20}	3.24	3.39×10^{-6}
$26s_{1/2}$	$8d_{3/2}$	$M1, E2$	0.006	1.59×10^{-19}	2.00	2.68×10^{-3}
$25d_{3/2}$	$8d_{3/2}$	$M1, E2$	0.004	4.17×10^{-19}	1.98	1.91×10^{-4}
$25d_{5/2}$	$8d_{3/2}$	$M1, E2$	0.003	6.77×10^{-20}	1.95	3.69×10^{-5}

FIGURE 2
(A) Isomeric excitation cross sections of ^{229}Th$^{1+,2+,3+}$ ions through NEEC. For each ionic state, the largest 10 NEEC channels are shown. The inset zooms in a small energy range around 2.38 eV. **(B)** The corresponding resonant strengths S.

eV. From Table 1, Table 2, and Table 3 one can see the spontaneous emission rate usually being on the order of 10^{-8} eV. Note that the importance of a NEEC channel is not only determined by the peak height, but also determined by the peak width, or the rate Γ_{NEEC}. After integrating over energy, we have the resonant strength S as shown in Figure 2B. The resonant strengths of these dominant

channels are on the order of 10^{-4} to 1 b·eV. The cross section and the resonant strength help us to identify the dominant NEEC channels.

In real calculations, it is often found that the S values of some channels are several orders of magnitude larger than other channels. Figure 3A shows the resonant strengths of different channels

FIGURE 3
(A) NEEC resonant strengths S for captures into ns, np, nd electronic states of the ^{229}Th^{1+} ion as a function of the free-electron energy. **(B)** Radial matrix element M_{fi} of partial wave transition channels when the free electron is captured into different bound states.

FIGURE 4
NEIES cross section of ^{229}Th nucleus for different ion-core potentials, as labeled.

captured into electronic states with different principal quantum numbers and orbital angular momenta. When the principal quantum number increases, the resonant strength decreases. And when the orbital angular momentum increases, the resonant strength decreases exponentially. The reason is that the radial matrix element in Eqs 27 and 31 decreases rapidly with the increase of n and l. Figure 3B shows the radial matrix element M_{fi} as a function of the integral upper limit r. When the final state is $7s_{1/2}$, M_{fi} is lager than that of $10s_{1/2}$ and $7d_{3/2}$, and the value of M_{fi} converges where r is very small (usually smaller than 0.1 a. u.). This means that the wave function close to the nucleus is dominant. These phenomena are caused by the change of the radial wave function with n and l. For the final state of electron, the larger the n and l, the farther away the electron from the nucleus, the smaller the amplitude of the wave function near the nucleus. For the initial state of electron, partial-wave components with small angular momenta are more appreciably distorted [32, 36]. Therefore, the amplitudes of

the partial wave with large angular momenta are much smaller than that with $l = 0$.

3.3 NEIES cross section

The NEIES process has been discussed in detail previously, for ^{229}Th [31, 32] and ^{235}U [51]. Here we just mention it briefly.
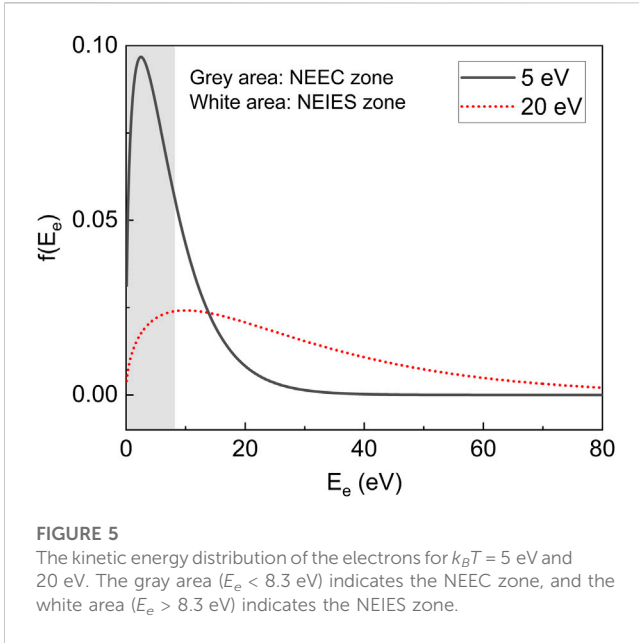
Figure 4 displays the NEIES cross sections for different ion-core potentials. Three cases have been shown, namely, the neutral ^{229}Th atom, the bare nucleus ^{229}Th^{90+}, and without the ion-core potential [i.e., $\mathcal{V}(r) = 0$ in Eq. 9]. When the ion-core potential is taken into account, the wave function in Eq. 14 is a distorted wave. When the ion-core potential is ignored, the wave function in Eq. 14 is a plane wave. It can be seen from Figure 4 that for the distorted wave, the cross sections are on the order of 10^{-3} to 10^{-2} b for electron energies around 10 eV. Then the cross section decreases gradually with the increase of the electron energy. Besides, there is no significant difference between the neutral ^{229}Th and the ^{229}Th^{90+} (except around 10 eV), telling that the cross section has a very weak ionic-state dependency. For the plane wave, however, the cross section is smaller by several orders of magnitude. This is due to the failure for the plane wave to describe the behavior of the electron wave function near the nucleus [32].

3.4 Isomer excitation in plasmas

In this section, we consider isomer excitation via the above-explained electronic processes in plasmas, which are assumed to be in thermal equilibrium. The distribution of ionic states can be estimated using the Saha equation [77, 78]

$$\frac{n_{i+1}^j}{n_i^k} = \frac{2g_j}{g_k} \frac{(2\pi m_e k_B T)^{3/2}}{(2\pi h)^3 n_e} e^{-\frac{\epsilon_{jk}}{k_B T}}, \qquad (39)$$

where n_i^k designates the number density of the ions with charge i and in the k-th electronic state, and n_e is the number density of free electrons. g_k is the degeneracy of the k state. k_B is the Boltzmann

FIGURE 5
The kinetic energy distribution of the electrons for $k_B T$ = 5 eV and 20 eV. The gray area ($E_e < 8.3$ eV) indicates the NEEC zone, and the white area ($E_e > 8.3$ eV) indicates the NEIES zone.

constant, T is the plasma temperature. ϵ_{jk} is the energy required to go from state j to k.

The rate of exciting a single ^{229}Th nucleus in the plasma is

$$\mathcal{W} = \mathcal{W}_{\text{NEET}} + \mathcal{W}_{\text{NEEC}} + \mathcal{W}_{\text{NEIES}}$$

$$= \sum_{ij} P_i^j \omega_{\text{NEET}}^{ij} + n_e \int dE_e \ f(E_e) v_e \sum_i P_i \left[\sigma_{\text{NEEC}}^i (E_e) + \sigma_{\text{NEIES}}^i (E_e) \right],$$

(40)

where P_i^j is the probability of an atom in ionic state i and electronic state j, calculated by Eq. 39. $\omega_{\text{NEET}}^{ij}$ is the corresponding NEET rate. $P_i = \sum_j P_i^j$ is the total probability of ionic state i. $f(E_e)$ is the normalized distribution function of the electron kinetic energy. Under thermal equilibrium, $f(E_e)$ follows the Maxwell-Boltzmann distribution, as shown in Figure 5. v_E is the velocity of the free electron.

Example results are shown in Table 4 for two different temperatures (5 eV, 20 eV) and two different electron densities (10^{16} cm^{-3}, 10^{20} cm^{-3}). Under these conditions, $\mathcal{W}_{\text{NEET}}$ is on the order of $10^{-5} - 10^{-4}$ s^{-1}, significantly lower than $\mathcal{W}_{\text{NEEC}}$ and $\mathcal{W}_{\text{NEIES}}$. This is because in plasmas, the probability of the electron being in the required ϕ_i is low, i.e., P_i^j is small. Meanwhile, $\mathcal{W}_{\text{NEET}}$ does not dependent appreciably on plasma parameters.

In contrast, NEEC and NEIES processes depend more sensitively on the plasma parameters because their initial states are free states. Whether NEEC or NEIES dominates depends on the temperature. For example, at $k_B T = 5$ eV, $\mathcal{W}_{\text{NEEC}} > \mathcal{W}_{\text{NEIES}}$ but at

$k_B T = 20$ eV, $\mathcal{W}_{\text{NEEC}} < \mathcal{W}_{\text{NEIES}}$. This is because at different temperatures the kinetic energy distribution favors different processes [79]. From Figure 5 one can see that the lower temperature has more proportion in the NEEC zone while the higher temperature has more proportion in the NEIES zone.

4 Further remarks

(a) Note that the NEET rates given in Sec 3.1 are based on the assumption that the ion has been prepared in the desired excited state ϕ_i. However, one needs to keep in mind that it may not be an easy task to prepare a specific ionic excited state. As shown in Sec 3.4, in plasma environments NEET is usually less efficient than NEEC or NEIES. An experimental environment that can more precisely control the ion excited state may favor the NEET process, such as an electron beam ion trap [80].

One should also bear in mind that the energy of the ^{229}Th isomer is only known with an uncertainty of 0.17 eV, which may result in an underestimation or overestimation of the calculated NEET rate. This uncertainty may lead to an uncertainty of about 1–4 orders of magnitude in the NEET rate. However, without a more precise determination of the isomeric energy, little can be done further, except for more precise calculations of the electronic structure and listing out possible NEET channels based on the current value of the isomeric energy.

(b) The NEEC process mostly occurs with free-electron energies within the range $(0, E_{\text{is}})$ because the final state of the electron is a bound state with a negative energy. Rare exceptions might exist if the final state is a bound state within the continuum, for example, a doubly excited state. These exceptions are beyond the scope of the current study, but might worth an investigation.

(c) The NEIES process can be realized more straightforwardly by using an external electron beam with electron energies tuned to values corresponding to the highest excitation cross sections, i.e., around 10 eV from Figure 4.

(d) Parallel to these nuclear-excitation processes are a few atomic processes, including electron-impact ionization, electron-impact atomic excitation, and radiative recombination. The cross section of electron-impact ionization is usually on the order of 10^{-16} cm^2 [81]. The cross section of electron-impact atomic excitation is usually on the order of 10^{-19} cm^2 [81]. And the cross section of radiative recombination is usually between 10^{-18} to 10^{-23} cm^2 [82]. They are at least several orders of magnitude stronger than the nuclear excitation processes and

TABLE 4 Rate of exciting a single ^{229}Th nucleus via NEET, NEEC, and NEIES in plasma conditions.

$k_B T$ (eV)	n_e (cm^{-3})	$\mathcal{W}_{\text{NEET}}$ (s^{-1})	$\mathcal{W}_{\text{NEEC}}$ (s^{-1})	$\mathcal{W}_{\text{NEIES}}$ (s^{-1})	$\mathcal{W}$ (s^{-1})
5	10^{16}	9.20×10^{-4}	0.013	0.003	0.016
5	10^{20}	9.76×10^{-4}	122.29	30.42	152.7
20	10^{16}	1.17×10^{-5}	0.002	0.005	0.007
20	10^{20}	1.46×10^{-4}	19.76	52.28	72.03

little interference is expected between the atomic processes and the nuclear-excitation processes [83].

5 Conclusion

In this paper, we consider nuclear excitation of ^{229}Th from the ground state to the low-lying isomeric state via electronic processes including NEET, NEEC and NEIES. We present a unified theoretical framework for the three processes with formulas for the excitation rate and the excitation cross section. These three processes are usually discussed separately for different nuclei, and we believe that a unified theoretical framework is helpful and useful for the general reader in this community. We emphasize that this is the first time the NEET and NEEC processes of ^{229}Th are investigated, although the accuracy of the NEET rates are limited by the current uncertainty in the isomeric energy. Detailed numerical results are presented which can be used directly in future studies.

Data availability statement

The original contributions presented in the study are included in the article/Supplementary Material, further inquiries can be directed to the corresponding author.

Author contributions

HZ and XW contributed to this work from four aspects. 1) HZ performed the formula derivation. 2) HZ and XW performed the analysis

of numerical results. 3) HZ wrote the first draft of the manuscript. 4) XW assisted with the discussion and revised the article. All authors contributed to the article and approved the submitted version.

Funding

Acknowledgments

Conflict of interest

The authors declare that the research was conducted in the absence of any commercial or financial relationships that could be construed as a potential conflict of interest.

Publisher's note

All claims expressed in this article are solely those of the authors and do not necessarily represent those of their affiliated organizations, or those of the publisher, the editors and the reviewers. Any product that may be evaluated in this article, or claim that may be made by its manufacturer, is not guaranteed or endorsed by the publisher.

References

1. Kroger LA, Reich CW. Features of the low-energy level scheme of ^{229}Th as observed in the α-decay of ^{233}U. *Nucl Phys A* (1976) 259:29–60. doi:10.1016/0375-9474(76)90494-2

2. Reich CW, Helmer RG. Energy separation of the doublet of intrinsic states at the ground state of ^{229}Th. *Phys Rev Lett* (1990) 64:271–3. doi:10.1103/PhysRevLett.64.271

3. Helmer RG, Reich CW. An excited state of ^{229}Th at 3.5 eV. *Phys Rev C* (1994) 49:1845–58. doi:10.1103/PhysRevC.49.1845

4. Beck BR, Becker JA, Beiersdorfer P, Brown GV, Moody KJ, Wilhelmy JB, et al. Energy splitting of the ground-state doublet in the nucleus ^{229}Th. *Phys Rev Lett* (2007) 98:142501. doi:10.1103/PhysRevLett.98.142501

5. Seiferle B, von der Wense L, Bilous PV, Amersdorffer I, Lemell C, Libisch F, et al. Energy of the ^{229}Th nuclear clock transition. *Nature* (2019) 573:243–6. doi:10.1038/s41586-019-1533-4

6. Huizenga J, Rao C, Engelkemeir D. 27-minute isomer of ^{235}U. *Phys Rev* (1957) 107:319–20. doi:10.1103/PhysRev.107.319

7. Freedman MS, Porter FT, Wagner F, Jr, Day P. Transition in 26-min ^{235m}U of less than 23 electronvolts. *Phys Rev* (1957) 108:836–41. doi:10.1103/PhysRev.108.836

8. Browne E, Tuli J. Nuclear data sheets for A = 235. *Nucl Data Sheets* (2014) 122:205–92. doi:10.1016/j.nds.2014.11.002

9. Pauli W Zur frage der theoretischen deutung der satelliten einiger spektrallinien und ihrer beeinflussung durch magnetische felder. *Naturwissenschaften* (1924) 12:741–3. doi:10.1007/BF01504828

10. Peik E, Tamm C. Nuclear laser spectroscopy of the 3.5 eV transition in ^{229}Th. *EPL* (2003) 61:181–6. doi:10.1209/epl/i2003-00210-x

11. Rellergert WG, DeMille D, Greco RR, Hehlen MP, Torgerson JR, Hudson ER. Constraining the evolution of the fundamental constants with a solid-state optical frequency reference based on the ^{229}Th nucleus. *Phys Rev Lett* (2010) 104:200802. doi:10.1103/PhysRevLett.104.200802

12. Campbell CJ, Radnaev AG, Kuzmich A, Dzuba VA, Flambaum VV, Derevianko A. Single-ion nuclear clock for metrology at the 19th decimal place. *Phys Rev Lett* (2012) 108:120802. doi:10.1103/PhysRevLett.108.120802

13. Tkalya EV. Proposal for a nuclear gamma-ray laser of optical range. *Phys Rev Lett* (2011) 106:162501. doi:10.1103/PhysRevLett.106.162501

14. Flambaum VV. Enhanced effect of temporal variation of the fine structure constant and the strong interaction in ^{229}Th. *Phys Rev Lett* (2006) 97:092502. doi:10.1103/PhysRevLett.97.092502

15. Berengut JC, Dzuba VA, Flambaum VV, Porsev SG. Proposed experimental method to determine α sensitivity of splitting between ground and 7.6 eV isomeric states in ^{229}Th. *Phys Rev Lett* (2009) 102:210801. doi:10.1103/PhysRevLett.102.210801

16. Fadeev P, Berengut JC, Flambaum VV. Sensitivity of ^{229}Th nuclear clock transition to variation of the fine-structure constant. *Phys Rev A* (2020) 102:052833. doi:10.1103/PhysRevA.102.052833

17. Verlinde M, Kraemer S, Moens J, Chrysalidis K, Correia J, Cottenier S, et al. Alternative approach to populate and study the ^{229}Th nuclear clock isomer. *Phys Rev C* (2019) 100:024315. doi:10.1103/PhysRevC.100.024315

18. Jeet J, Schneider C, Sullivan ST, Rellergert WG, Mirzadeh S, Cassanho A, et al. Results of a direct search using synchrotron radiation for the low-energy ^{229}Th nuclear isomeric transition. *Phys Rev Lett* (2015) 114:253001. doi:10.1103/PhysRevLett.114.253001

19. Yamaguchi A, Kolbe M, Kaser H, Reichel T, Gottwald A, Peik E. Experimental search for the low-energy nuclear transition in ^{229}Th with undulator radiation. *New J Phys* (2015) 17:053053. doi:10.1088/1367-2630/17/5/053053

20. Stellmer S, Kazakov G, Schreitl M, Kaser H, Kolbe M, Schumm T. Attempt to optically excite the nuclear isomer in ^{229}Th. *Phys Rev A* (2018) 97:062506. doi:10.1103/PhysRevA.97.062506

21. von der Wense L, Seiferle B, Stellmer S, Weitenberg J, Kazakov G, Pálffy A, et al. A laser excitation scheme for ^{229m}Th. *Phys Rev Lett* (2017) 119:132503. doi:10.1103/PhysRevLett.119.132503

22. Masuda T, Yoshimi A, Fujieda A, Fujimoto H, Haba H, Hara H, et al. X-ray pumping of the ^{229}Th nuclear clock isomer. *Nature* (2019) 573:238–42. doi:10.1038/s41586-019-1542-3

23. Tkalya EV, Zherikhin AN, Zhudov VI. Decay of the low-energy nuclear isomer ^{229m}Th (3/2+, 3.5±1.0 eV) in solids (dielectrics and metals): A new scheme of experimental research. *Phys Rev C* (2000) 61:064308. doi:10.1103/PhysRevC.61.064308

24. Tkalya EV. Probability of nonradiative excitation of nuclei in transitions of an electron in an atomic shell. *Sov Phys JETP* (1992) 75:200–9.

25. Porsev SG, Flambaum VV. Electronic bridge process in ²²⁹Th⁺. *Phys Rev A* (2010) 81:042516. doi:10.1103/PhysRevA.81.042516

26. Porsev SG, Flambaum VV, Peik E, Tamm C. Excitation of the isomeric ²²⁹Th nuclear state via an electronic bridge process in ²²⁹Th⁺. *Phys Rev Lett* (2010) 105:182501. doi:10.1103/PhysRevLett.105.182501

27. Bilous PV, Peik E, Pálffy A. Laser-induced electronic bridge for characterization of the ²²⁹ᵐTh →²²⁹ᵍTh nuclear transition with a tunable optical laser. *New J Phys* (2018) 20: 013016. doi:10.1088/1367-2630/aa9cd9

28. Dzyublik AY. Excitation of ²²⁹ᵐTh in the electron bridge via continuum, as a scattering process. *Phys Rev C* (2020) 102:024604. doi:10.1103/PhysRevC.102.024604

29. Bilous PV, Bekker H, Berengut JC, Seiferle B, von der Wense L, Thirolf PG, et al. Electronic bridge excitation in highly charged ²²⁹Th ions. *Phys Rev Lett* (2020) 124: 192502. doi:10.1103/PhysRevLett.124.192502

30. Nickerson BS, Pimon M, Bilous PV, Gugler J, Beeks K, Sikorsky T, et al. Nuclear excitation of the ²²⁹Th isomer via defect states in doped crystals. *Phys Rev Lett* (2020) 125:032501. doi:10.1103/PhysRevLett.125.032501

31. Tkalya EV. Excitation of ²²⁹ᵐTh at inelastic scattering of low energy electrons. *Phys Rev Lett* (2020) 124:242501. doi:10.1103/PhysRevLett.124.242501

32. Zhang H, Wang W, Wang X. Nuclear excitation cross section of ²²⁹Th via inelastic electron scattering. *Phys Rev C* (2022) 106:044604. doi:10.1103/PhysRevC.106.044604

33. Tkalya EV Cross section of the coulomb excitation of by low energy muons. *Chin Phys C* (2021) 45:094102. doi:10.1088/1674-1137/ac0b3a

34. Wang W, Zhou J, Liu B, Wang X. Exciting the isomeric ²²⁹Th nuclear state via laser-driven electron recollision. *Phys Rev Lett* (2021) 127:052501. doi:10.1103/PhysRevLett.127.052501

35. Wang W, Zhang H, Wang X. Strong-field atomic physics meets ²²⁹Th nuclear physics. *J Phys B: Mol Opt Phys* (2022) 54:244001. doi:10.1088/1361-6455/ac45ce

36. Wang X. Nuclear excitation of ²²⁹Th induced by laser-driven electron recollision. *Phys Rev C* (2022) 106:024606. doi:10.1103/PhysRevC.106.024606

37. Morita M. Nuclear excitation by electron transition and its application to uranium 235 separation. *Prog Theor Phys* (1973) 49:1574–86. doi:10.1143/PTP.49.1574

38. Fujioka H, Ura K. Nanosecond stroboscopic electron spectroscopy for observation of nuclear excitation by electron transition (NEET) in ¹⁹⁷Au. *Jpn J Appl Phys* (1985) 24: 1703. doi:10.1143/JJAP.24.1703

39. Tkalya EV. Nuclear excitation in atomic transitions (NEET process analysis). *Nucl Phys A* (1992) 539:209–22. doi:10.1016/0375-9474(92)90267-N

40. Kishimoto S, Yoda Y, Seto M, Kobayashi Y, Kitao S, Haruki R, et al. Observation of nuclear excitation by electron transition in ¹⁹⁷Au with synchrotron X-rays and an avalanche photodiode. *Phys Rev Lett* (2000) 85:1831–4. doi:10.1103/PhysRevLett.85.1831

41. Sakabe S, Takahashi K, Hashida M, Shimizu S, Iida T. Elements and their transitions feasible for NEET. *Data Nucl Data Tables* (2005) 91:1–7. doi:10.1016/j.adt.2005.07.002

42. Goldanskii VI, Namiot VA. On the excitation of isomeric nuclear levels by laser radiation through inverse internal electron conversion. *Phys Lett B* (1976) 62:393–4. doi:10.1016/0370-2693(76)90665-1

43. Cue N. Nuclear excitation by target electron capture. *Nucl Instrum Methods Phys Res B* (1989) 40:25–7. doi:10.1016/0168-583X(89)90914-2

44. Yuan ZS, Kimball JC. First-principles calculation of the cross sections for nuclear excitation by electron capture of channeled nuclei. *Phys Rev C* (1993) 47:323–8. doi:10.1103/PhysRevC.47.323

45. Harston M, Chemin J. Mechanisms of nuclear excitation in plasmas. *Phys Rev C* (1999) 59:2462–73. doi:10.1103/PhysRevC.59.2462

46. Pálffy A, Scheid W, Harman Z. Theory of nuclear excitation by electron capture for heavy ions. *Phys Rev A* (2006) 73:012715. doi:10.1103/PhysRevA.73.012715

47. Gunst J, Litvinov YA, Keitel CH, Pálffy A. Dominant secondary nuclear photoexcitation with the X-ray free-electron laser. *Phys Rev Lett* (2014) 112:082501. doi:10.1103/PhysRevLett.112.082501

48. Chiara C, Carroll J, Carpenter M, Greene J, Hartley D, Janssens R, et al. Isomer depletion as experimental evidence of nuclear excitation by electron capture. *Nature* (2018) 554:216–8. doi:10.1038/nature25483

49. Wu Y, Keitel CH, Pálffy A. ⁹³ᵐMo isomer depletion via beam-based nuclear excitation by electron capture. *Phys Rev Lett* (2019) 122:212501. doi:10.1103/PhysRevLett.122.212501

50. Guo S, Ding B, Zhou X, Wu Y, Wang J, Xu S, et al. Probing ⁹³ᵐMo isomer depletion with an isomer beam. *Phys Rev Lett* (2022) 128:242502. doi:10.1103/PhysRevLett.128.242502

51. Liu B, Wang X. Isomeric excitation of ²³⁵U by inelastic scattering of low-energy electrons. *Phys Rev C* (2022) 106:064604. doi:10.1103/PhysRevC.106.064604

52. Hofstadter R, Fechter HR, McIntyre JA. High-energy electron scattering and nuclear structure determinations. *Phys Rev* (1953) 92:978–87. doi:10.1103/PhysRev.92.978

53. Barber WC. Inelastic electron scattering. *Springer Tracts Mod Phys* (1962) 12: 1–42. doi:10.1146/annurev.ns.12.120162.000245

54. Rosen M, Raphael R, Überall H. Generalized helm model for transverse electroexcitation of nuclear levels. *Phys Rev* (1967) 163:927–34. doi:10.1103/PhysRev.163.927

55. Theissen H. Spectroscopy of light nuclei by low energy (¡ 70 MeV) inelastic electron scattering. *Springer Tracts Mod Phys* (1972) 65:1–57. doi:10.1007/BFb0041391

56. Donnelly TW, Walecka JD. Electron scattering and nuclear structure. *Annu Rev Nucl Sci* (1975) 25:329–405. doi:10.1146/annurev.ns.25.120175.001553

57. Bertrand FE. Excitation of giant multipole resonances through inelastic scattering. *Annu Rev Nucl Sci* (1976) 26:457–509. doi:10.1146/annurev.ns.26.120176.002325

58. Taylor RE. Deep inelastic scattering: The early years. *Rev Mod Phys* (1991) 63: 573–95. doi:10.1103/RevModPhys.63.573

59. Rose ME. *Relativistic electron theory*. New York: Wiley (1961).

60. Berestetskii VB, Lifshitz EM, Pitaevskii LP. *Quantum electrodynamics*, 4. Oxford: Butterworth-Heinemann (1982).

61. Alder K, Bohr A, Huus T, Mottelson B, Winther A. Study of nuclear structure by electromagnetic excitation with accelerated ions. *Rev Mod Phys* (1956) 28:432–542. doi:10.1103/RevModPhys.28.432

62. Abramowitz M, Stegun IA. *Handbook of mathematical functions with formulas, graphs, and mathematical tables*, 55. Washington: US Government printing office (1964).

63. Blin-Stoyle R. Theory of complex nuclei. *Phys Bull* (1977) 28:131. doi:10.1088/0031-9112/28/3/058

64. Aas AJ, Mach H, Borge MJG, Fogelberg B, Grant IS, Gulda K, et al. Enhanced and quenched B(E1) transition rates between parity doublet bands in ²²⁷Ra. *Nucl Phys A* (1996) 611:281–314. doi:10.1016/S0375-9474(96)00312-0

65. Bemis CE, McGowan FK, Ford JLC, Jr, Milner WT, Robinson RL, Stelson PH, et al. Coulomb excitation of states in ²²⁹Th. *Phys Scr* (1988) 38:657–63. doi:10.1088/0031-8949/38/5/004

66. Gulda K, Kurcewicz W, Aas AJ, Borge MJG, Burke DG, Fogelberg B, et al. The nuclear structure of ²²⁹Th. *Nucl Phys A* (2002) 703:45–69. doi:10.1016/S0375-9474(01)01456-7

67. Barci V, Ardisson G, Barci-Funel G, Weiss B, El Samad O, Sheline RK. Nuclear structure of ²²⁹Th from γ-ray spectroscopy study of ²³³U α-particle decay. *Phys Rev C* (2003) 68:034329. doi:10.1103/PhysRevC.68.034329

68. Ruchowska E, Płóciennik W, Żylicz J, Mach H, Kvasil J, Algora A, et al. Nuclear structure of ²²⁹Th. *Phys Rev C* (2006) 73:044326. doi:10.1103/PhysRevC.73.044326

69. Tkalya EV, Schneider C, Jeet J, Hudson ER. Radiative lifetime and energy of the low-energy isomeric level in ²²⁹Th. *Phys Rev C* (2015) 92:054324. doi:10.1103/PhysRevC.92.054324

70. Dykhne AM, Tkalya EV. ²²⁹ᵐTh (3/2+, 3.5 eV) and a check of the exponentiality of the decay law. *J Exp Theor Phys* (1998) 67:549–52. doi:10.1134/1.567724

71. Minkov N, Pálffy A. Reduced transition probabilities for the gamma decay of the 7.8 eV isomer in ²²⁹Th. *Phys Rev Lett* (2017) 118:212501. doi:10.1103/PhysRevLett.118.212501

72. Salvat F, Fernandez-Varea JM. Radial: A fortran subroutine package for the solution of the radial Schrödinger and Dirac wave equations. *Comput Phys Commun* (2019) 240:165–77. doi:10.1016/j.cpc.2019.02.011

73. Liberman DA, Waber JT, Cromer DT. Self-Consistent-field Dirac-slater wave functions for atoms and ions. I. Comparison with previous calculations. *Phys Rev* (1965) 137:A27–34. doi:10.1103/PhysRev.137.A27

74. Liberman DA, Cromer DT, Waber JT. Relativistic self-consistent field program for atoms and ions. *Comput Phys Commun* (1971) 2:107–13. doi:10.1016/0010-4655(71)90020-8

75. Seiferle B, von der Wense L, Thirolf P G Lifetime measurement of the ²²⁹Th nuclear isomer. *Phys Rev Lett* (2017) 118:042501. doi:10.1103/PhysRevLett.118.042501

76. Borisyuk PV, Chubunova EV, Kolachevsky NN, Lebedinskii YY, Vasiliev OS, Tkalya EV. *Excitation of ²²⁹Th nuclei in laser plasma: The energy and half-life of the low-lying isomeric state*. arXiv [Preprint] (2018). Available at: http://arxiv.org/abs/1804.00299v1 (Accessed April 1, 2018).

77. Griem HR. *Principles of plasma spectroscopy*. Cambridge: Cambridge University Press (1997).

78. Drake RP. *High-energy-density physics*. Berlin: Springer (2010).

79. Qi J, Zhang H, Wang X. Isomeric excitation of ²²⁹Th in laser-heated clusters. *Phys Rev Lett* (2023) 130:112501. doi:10.1103/PhysRevLett.130.112501

80. Levine MA, Marrs RE, Henderson JR, Knapp DA, Schneider MB. The electron beam ion trap: A new instrument for atomic physics measurements. *Phys Scr* (1988) 1988:157–63. doi:10.1088/0031-8949/1988/T22/024

81. National Institute of Standards and Technology Physical Measurement Laboratory. *Atomic reference data for electronic structure calculations* (2001). Available at: https://physics.nist.gov/PhysRefData/Ionization/atom_index.html.

82. Ichihara A, Eichler J. Cross sections for radiative recombination and the photoelectric effect in the K, L, and M shells of one-electron systems with 1 ≤ Z ≤ 112 calculated within an exact relativistic description. *Data Nucl Data Tables* (2000) 74: 1–121. doi:10.1006/adnd.1999.0825

83. Pálffy A, Harman Z, Scheid W. Quantum interference between nuclear excitation by electron capture and radiative recombination. *Phys Rev A* (2007) 75:012709. doi:10.1103/PhysRevA.75.012709